Published in final edited form as:
Bone. 2010 June ; 46(6): 1582–1590. doi:10.1016/j.bone.2010.02.020.

Quantitative ^{31}P NMR Spectroscopy and ^{1}H MRI Measurements of Bone Mineral and Matrix Density Differentiate Metabolic Bone Diseases in Rat Models

Haihui Cao[1,3,7], **Ara Nazarian**[2,7], **Jerome L. Ackerman**[1,3,4,7], **Brian D. Snyder**[1,2,7], **Andrew E. Rosenberg**[5,7], **Rosalynn M. Nazarian**[5,7], **Mirko I. Hrovat**[6], **Guangping Dai**[3,7], **Dionyssios Mintzopoulos**[3,7], and **Yaotang Wu**[1,3,7,*]

[1] Department of Orthopaedic Surgery, Children's Hospital, Boston, MA 02115

[2] Center for Advanced Orthopaedic Studies, Department of Orthopaedic Surgery, Beth Israel Deaconess Medical Center, Boston, MA 02215

[3] Martinos Center for Biomedical Imaging, Department of Radiology, Massachusetts General Hospital, Charlestown, MA 02129

[4] Harvard-MIT Division of Health Sciences and Technology, Cambridge, MA 02139

[5] Department of Pathology, Massachusetts General Hospital, Boston, MA 02114

[6] Mirtech, Inc., Brockton, MA 02301

[7] Harvard Medical School, Boston, MA 02115

Abstract

In this study, bone mineral density (BMD) of normal (CON), ovariectomized (OVX) and partially nephrectomized (NFR) rats was measured by ^{31}P NMR spectroscopy; bone matrix density was measured by ^{1}H water- and fat-suppressed projection imaging (WASPI); and the extent of bone mineralization (EBM) was obtained by the ratio of BMD/bone matrix density. The capability of these MR methods to distinguish the bone composition of the CON, OVX and NFR groups was evaluated against chemical analysis (gravimetry). For cortical bone specimens, BMD of the CON and OVX groups was not significantly different; BMD of the NFR group was 22.1% (by ^{31}P NMR) and 17.5% (by gravimetry) lower than CON. For trabecular bone specimens, BMD of the OVX group was 40.5% (by ^{31}P NMR) and 24.6% (by gravimetry) lower than CON; BMD of the NFR group was 26.8% (by ^{31}P NMR) and 21.5% (by gravimetry) lower than CON. No significant change of cortical bone matrix density between CON and OVX was observed by WASPI or gravimetry; NFR cortical bone matrix density was 10.3% (by WASPI) and 13.9% (by gravimetry) lower than CON. OVX trabecular bone matrix density was 38.0% (by WASPI) and 30.8% (by gravimetry) lower than CON, while no significant change in NFR trabecular bone matrix density was observed by either method. The EBMs of OVX cortical and trabecular specimens were slightly higher than CON but not significantly different from CON. Importantly, EBMs of NFR cortical and trabecular specimens were 12.4% and 26.3% lower than CON by ^{31}P NMR/WASPI, respectively; and 4.0% and 11.9% lower by gravimetry. Histopathology showed evidence of osteoporosis in the OVX group and severe secondary

Corresponding Author: Yaotang Wu, Department of Orthopaedic Surgery, Children's Hospital, Room 930, Enders Building, 300 Longwood Avenue, Boston, MA 02115, Phone: 617-919-2060, Fax: 617-730-0122, yaotang.wu@childrens.harvard.edu.

hyperparathyroidism (renal osteodystrophy) in the NFR group. These results demonstrate that the combined ^{31}P NMR/WASPI method is capable of discerning the difference in EBM between animals with osteoporosis and those with impaired bone mineralization.

Keywords

bone mineralization; MRI; WASPI; osteoporosis; osteomalacia

Introduction

According to the US Surgeon General's report on "Bone Health and Osteoporosis" released in 2004, there are roughly 10 million Americans over the age of 50 with osteoporosis. Additionally, another 34 million have low bone mass or "osteopenia" of the hip, which puts them at risk for osteoporosis, fracture, and the associated complications later in life [1].

Osteopenia is defined by the World Health Organization as having a bone mineral density (BMD) score between 1.0 and 2.5 standard deviations below the BMD of a normal young adult, and osteoporosis is defined as having a BMD lower than 2.5 standard deviations. In practice, BMD is measured by X-ray-based bone densitometry methods, such as Dual Energy X-ray Absorptiometry (DXA) and Quantitative and Peripheral X-ray Computed Tomography (QCT and pQCT) [2–5]. However, in addition to osteoporosis, other metabolic bone diseases can also result in low BMD [6–9].

In the case of osteoporosis, bone formation is not able to compensate for bone resorption, leading to thinning and loss of connectivity in trabecular bone and deep resorption cavities in cortical bone [10]. Studies and guidelines for diagnosis and management of osteoporosis have shown that even though the amount of mineral per unit volume of bone substance (mineral plus matrix) might not differ substantially from normal, the amount of mineral per unit volume of bone tissue (bone substance, bone cells, marrow, blood vessels and other soft tissues) is decreased. In other words, while the extent of mineralization (EBM) of osteoporotic bone may be close to normal, BMD of osteoporotic bone tissue is definitely low [9,11].

In the case of impaired bone mineralization, the osteoid thickness is increased and mineralization lag time is prolonged. Hence the amount of mineral per unit volume of bone substance is lower, and the amount of mineral per unit volume of bone tissue also is decreased, that is both the EBM and BMD are lower. The causes of impaired bone mineralization can be inadequate nutritional supply of vitamin D, calcium or phosphorus; renal failure; or interference of certain drugs with calcium and vitamin D metabolism [12].

The critical point is that measurement of BMD alone does not permit the physician to distinguish osteoporosis from impaired bone mineralization, which could result in treatment for the wrong condition.

At present, the best direct measurements of EBM are histomorphometric indices which can only be obtained invasively by bone biopsy [13]. Although serum vitamin D measurements can indicate that a mineralization defect is present, routine vitamin D blood testing frequently fails to detect the condition and cannot serve as a quantitative measure of EBM. There is an urgent need to develop new noninvasive methods that can measure not only BMD but bone matrix as well, and provide physicians with information on bone mineralization.

The broad resonance lines and very short spin-spin relaxation times (T_2) of the magnetic resonance signals of bone substance (^{31}P signal from mineral and ^{1}H signal from organic bone matrix) are the major obstacles for traditional MRI to image bone substance. New methods to

overcome these obstacles have been developed recently. Ultrashort echo time (UTE) MRI has been developed by Robson et al., Reichert et al., and Du et al. to image solid components of human bone [14–16]. More recently, a radial projection pulse sequence with long-T_2 soft tissue suppression has been developed by Techawiboonwong and co-workers to image the solid-like components of bone matrix [17]. Another approach to visualize short-T_2 hard tissues, sweep imaging with Fourier transformation (SWIFT), has been developed by Idiyatullin and co-workers, in which magnetic resonance time-domain signals are acquired during a swept RF excitation in a timeshared manner [18]. Anumula, et al., first investigated hypomineralization by ^{31}P solid-state MRI [19], and later by ^{1}H and ^{31}P solid-state MRI [20].

Our group has been engaged in developing ^{31}P solid-state magnetic resonance imaging (SMRI) to visualize bone mineral [21–23], and quantitative water- and fat-suppressed proton projection MRI (WASPI) to visualize solid bone matrix [24–26]. With these new methods, MRI measurements of bone mineral and matrix density have become available. These two methods emphasize a pair of key features that ensure the quantitative accuracy of the intensity of the solid state signals: (a) the use of very short duration (~10 μs) hard RF excitation pulses that uniformly excite large spectral bandwidths, and (b) minimal delay (also ~10 μs) between the end of the RF pulse and the beginning of data acquisition. These constraints require that no magnetic field gradient is switched in the interval from the start of the RF pulse to the end of data acquisition. Therefore, when imaging is performed the excitation pulse is applied during a constant amplitude gradient pulse, and the image is reconstructed from free induction decays (FIDs) [22].

The purpose of this study is to assess the validity of ^{31}P measurement of bone mineral content and ^{1}H measurement of bone matrix content in rat models of reduced total bone density and reduced mineralization by comparison with gravimetric analysis. Because the size of rat bone specimens is small enough to be placed well within the effective volume of the MRI coil, single pulse ^{31}P spectroscopy was utilized to measure the total mineral content. WASPI ^{1}H solid state MRI was used to measure the matrix content. Reduced total bone was obtained with the ovariectomized (OVX) rat model, which has been widely used to study the effects of menopause on bone mass, trabecular microstructure, and fracture risk and to model human osteoporosis [27–35]. Reduced mineralization is achieved with the partially nephrectomized (NFR) rat model, which has been used to study the effects of renal osteodystrophy on bone metabolism [36–42].

Materials and methods

Animal model and specimen preparation

Thirty mature female Sprague Dawley (SD) rats (250–275 g, ~15 weeks old) were obtained from Charles River Laboratories (Charles River, Charlestown, MA, USA) and were divided into three equally sized groups: the animals in the control group (CON) were not subjected to any surgical or dietary interventions. The OVX group underwent bilateral ovariectomy at the animal supplier's facility 1 week prior to arrival in the laboratory to induce a state of low bone mass and micro-architectural deterioration. The NFR group underwent 5/6 nephrectomy at the animal supplier's facility one week prior to arrival in the laboratory. Additionally, on arrival in the laboratory the NFR animals were placed on a modified diet containing 0.6% Ca and 1.2% P for the duration of the experiment. Normal rodent diet contains 1.35% Ca and 1.04% P. These two conditions to which the NFR animals were subjected induce renal osteodystrophy and severe secondary hyperparathyroidism. The animals were euthanized via CO_2 inhalation 8, 10 and 12 weeks after arriving at the laboratory for CON, OVX and NFR groups respectively, and one femur (selected at random) per animal was used for the study.

After dissection and cleaning of all adherent soft tissues, a mid-diaphyseal (cortical bone only) and a distal metaphyseal (trabecular + cortical bone) segment was cut from each femur perpendicular to the anatomical axis between two parallel diamond wafering blades on a low-speed saw (Isomet, Buehler Corporation, Lake Bluff, IL, USA) under copious irrigation. The cortical midshaft segments (height 5.99 ± 0.28 mm, diameter 3.64 ± 0.24 mm) were cut to maintain an approximate 2:1 height to diameter ratio, while the distal metaphyseal segments (height 6.22 ± 0.73 mm, diameter 4.84 ± 0.41 mm), with the thin cortex shaved off, were cut immediately above the growth plate to include the distal metaphyseal trabecular structure. The metaphyseal cortex was shaved off under an established protocol, detailed elsewhere [43], using diamond wafering blades and optical magnification.

The study protocol was approved by Beth Israel Deaconess Medical Center's Institutional Animal Care and Use Committee (IACUC), and carried out in the Center for Advanced Orthopaedic Studies, Department of Orthopaedic Surgery, Beth Israel Deaconess Medical Center, Boston.

NMR and MRI measurements

NMR and MRI data were obtained with a Bruker 4.7 T 33 cm bore scanner equipped with a 400 mT/m gradient system (Bruker Biospin, Billerica, MA, USA) and a home-made RF probe with a 15 mm ID solenoid coil at room temperature. The ^{1}H and ^{31}P Larmor frequencies were 200.13 and 81.1 MHz respectively.

Spin-lattice relaxation time measurements

Proton and phosphorus T_1 measurements were carried out using a series of progressive-saturation experiments. For proton measurements, the projection gradient was applied only in the z-direction, resulting in a 1D WASPI to ensure that the signal arises from the components of interest while reducing the total experiment time. Single pulse ^{31}P spectroscopy of the entire bone was performed for ^{31}P T_1 measurements. The signal was averaged over 128 scans for proton and 1280 scans for ^{31}P, and the experiment repetition time (*TR*) varied from 0.1 s to 10 s. The measured signal amplitudes M were fitted to the Ernst equation for the magnetization M [44] using three fitting parameters M_0, β, and T_1

$$M = M_0(1 - \exp(-TR/T_1))(\sin\beta)/(1 - (\cos\beta)\exp(-TR/T_1)) \quad (1)$$

where M_0 is the initial magnetization, and β is the excitation angle.

Bone matrix density measurement by WASPI

The water and fat suppressed proton projection MRI (WASPI) method has been described in detail [24–26]. In this study, WASPI data was acquired under the following protocol. The water and fat suppression pulses were 2–2.5 ms long, followed by an excitation RF pulse of 8 μs duration (14°). The MR data were acquired under fixed 160 mT/m gradient magnitudes at a sampling rate of 5 μs per complex point. The direction of the gradient varied from one projection to the next. The total number of directions was 2934, which generated 30 independent pixels across the 18 mm FOV, resulting in an image resolution of 0.6 mm. The receiver dead time was 10 μs. The experiment repetition time *(TR)* was 0.15 s and 16 acquisitions were averaged for each projection. A second data set was acquired with weaker gradients (80 mT/m), fewer directions (20), and longer dwell time (10 μs) to recover the data points lost in the receiver dead time, which corresponded to the data points close to the origin of the k space [25]. The total measurement time was approximately 2 h including both the first and the second sets of acquisitions.

Three cylindrical pellets of 20% poly(ethylene oxide) (PEO)/80% poly(methyl methacrylate) (PMMA) polymer blend powder (PEO from Sigma-Aldrich, St. Louis, MO, USA; PMMA from Scientific Polymer Products Ontario, NY, USA) diluted with silicon dioxide (quartz sand, 40–100 mesh, Fisher Scientific, Waltham, MA, USA) were formed by uniaxial compression in a hydraulic press (Carver, Wabash, IN, USA). The pellet densities were 1.17, 0.80, and 0.56 g of polymer per cubic centimmeter. The pellets served as a density calibration phantom (denoted below as the "polymer phantom"). Bone marrow/fat, obtained from the long bones of 2- to 3-month-old pigs (Animal Facility, Children's Hospital, Boston, MA, USA) shortly after sacrifice, was placed into small glass tubes to serve as a reference for water and fat suppression (denoted below as the "marrow tube").

A tube of aqueous $MnSO_4$ (~10 mmol/L, T_2~1 ms) was imaged to calibrate the ^1H image intensity over the measurement volume to compensate for spatial variations in the radiofrequency field strength produced by the RF coil.

In the non-suppression MR images, the total number of voxels of the bone specimen represents the total volume of bone tissue (*TV*) because bone tissue comprises the bone substance, marrow, and other soft tissues which can all be seen in the non-suppression MRI. It should be noted that the bone tissue volume *TV* of cortical bone specimens we measured from non-suppression MRI does not include the volume of medullary cavity spaces, while the measured *TV* of trabecular bone specimens includes the fluid-filled pores. The volume of the whole 3D image in terms of real physical units (cubic centimeter) is $(FOV)^3$. There are 64^3 voxels in that volume (the image reconstruction matrix is 64*64*64), so each voxel represents a real physical volume of $(FOV/64)^3$. Bone voxels in the non-suppression MR image were identified by selecting all voxels whose intensity was above a threshold, and the number of the selected voxels was multiplied by the conversion factor: $(FOV/64)^3$ to obtain the true *TV* volume in cm^3.

In WASPI images, the soft tissue signals are suppressed and only the signals from solid bone matrix (collagen, tightly bound water, and other immobile molecules) can be visualized. In practice, the individual polymer phantom pellet was identified by selecting all voxels whose intensity was at least 12 times the averaged background intensity. For each pellet *i* the WASPI derived polymer phantom density D_{cwi} (in units of intensity per voxel) was determined by dividing the sum of the voxel intensities by the total number of voxels in the pellet. A calibration curve for each WASPI image was created by plotting D_{cwi} of pellet *i* vs. its physical mass density D_{cpi} (the weight of the phantom/the volume of the phantom, in units of polymer $g.cm^{-3}$) for the three pellets, and fitting the three points with a linear regression. The bone matrix image density of the specimen D_{BmW} (in units of intensity per voxel) was determined by dividing the sum of the WASPI voxel intensities by *TV* of the same specimen. D_{BmW} was converted to polymer equivalent mass density D_{BmP} (in units of polymer $g.cm^{-3}$) using the linear regression parameters. By scanning each specimen with the polymer phantom and computing the calibration for each image, scan to scan instability or small changes in the scanner or pulse sequence settings do not corrupt the measurements. The polymer equivalent mass density D_{BmP} was then converted to true bone matrix mass density D_{WmaT} (in units of $g.cm^{-3}$) by applying a conversion factor obtained from the comparison of these two densities of bone samples in a previous WASPI/gravimetric analysis study [26]: the true bone matrix mass density $D_{WmaT} = 0.45\ D_{BmP}$ (polymer equivalent mass density).

Bone mineral density measurement by ^{31}P spectroscopy

Since the ^{31}P MR signal of a well cleaned bone specimen arises overwhelmingly from the mineral and the whole bone specimen was placed within the effective volume of the NMR coil, imaging is not required to insure that the acquired ^{31}P signal corresponds to the mineral content of a certain volume of the bone specimen as long as the bone specimen volume is known. Therefore single pulse ^{31}P spectroscopy was used to measure the total mineral content of the

whole specimen. A phosphorus intensity standard, a 4-mm diameter tube filled with 0.1407g (7.644×10^{-4} mole) KPF_6, was used to permit the conversion of signal intensity to mineral content in grams. Each bone specimen was placed alongside the KPF_6 tube and measured with single pulse ^{31}P spectroscopy (excitation pulse: $\beta = 20°$; *TR*: 1s). The ^{31}P chemical shift of KPF_6 is about 150 ppm downfield from the PO_4 resonance of bone mineral. The mineral and KPF_6 resonances do not overlap in the spectra. The true total bone mineral signal at infinite *TR* was obtained by multiplying the measured signal with a correction factor *F* calculated from the measured T_1 value and the acquisition parameters,

$$F=(1-(\cos\beta)\exp(-TR/T_1))/((1-\exp(-TR/T_1))(\sin\beta)) \quad (2)$$

The number of moles of phosphorus in bone mineral phosphorus was obtained by comparing the T_1 corrected bone signal with that of the KPF_6, which was further converted to the total mass of bone mineral by using the molecular mass of hydroxyapatite (HA). Finally, the bone mineral density (gram of HA per cubic centimeter of bone tissue) was calculated as the mass of bone mineral divided by the tissue volume *TV*.

Gravimetric analysis

A sonic agitator was used to remove the marrow and fat from the intramedullary canal and pore spaces of each specimen. Residual marrow and surface water were removed using a centrifuge (8000 G for 15 min). To determine the dry bone substance mass, each defatted and dewatered specimen was placed in a tared porcelain crucible and dried in an oven at 75°C for 24 hours to remove all but the most tightly bound water and then weighed. To determine the ash weight, each specimen was ashed in the same crucible at 600°C to burn off the organic matrix. The specimen was weighed every 24 hours over a 96 hour interval until no change in mass was observed. The tissue mineral density was calculated as the mass of ash divided by the volume of bone tissue *TV*. The tissue matrix density was calculated as (dry bone mass – ash mass)/*TV*.

Histology

Histologic evaluation of the morphologic differences in the bone specimens was performed. Bone specimens were fixed in 10% buffered formaldehyde for 24 hours and then decalcified for 3 hours using a 10 % hydrochloric acid solution. The decalcified specimens were rinsed in a normal saline solution and submitted in individual cassettes for tissue processing and paraffin embedding. The blocks were cut into 5 μm thick coronal sections using a microtome and mounted on protein-coated glass slides. The slides were then stained with hematoxylin and eosin (H&E), and microscopic evaluation was performed in a double-blinded fashion. Changes in the appearance of cortical and cancellous bone and ossification patterns were studied. Specifically, the morphologic composition of bone (cellular and organic components) and evidence of bone remodeling (osteoclastic bone resorption, woven bone formation) were assessed.

Statistical analysis

The bone mineral and matrix density data were assessed for normality using the Shapiro-Wilks test. Statistical calculations were performed with SPSS 12 (SPSS Inc, Chicago, IL) and with R 2.9.1 (http://www.r-project.org). Statistical comparisons between the test groups were performed with the unpaired two-tailed t-test. All results were expressed as mean ± SD. A *p* value less than 0.05 was considered statistically different.

Results

The spin-lattice relaxation time T_1 (^{1}H of rat bone matrix, ^{1}H of polymer blend, and ^{31}P of rat bone mineral, HA, KPF_6) was measured and is listed in Table 1. The results show that the proton T_1 of the polymer blend was very similar to that of solid bone matrix. Based on the T_1 values and excitation angles, a *TR* of 0.15 s was chosen in the following WASPI measurements of bone matrix. The correction factors *F* under these experimental conditions were calculated using equation 2. The *F* values of the bone specimen and polymer phantom was very close, with the difference being about 4% (Table 1). Therefore, no proton T_1 correction was needed. The ^{31}P T_1 of the bone specimens were much longer than that of KPF_6, which serves as calibration reference. The correction factors *F* were calculated for each group with *TR* = 1 s and flip angle β (Table 1). The long ^{31}P T_1 of bone mineral necessitated correction for T_1 effects using the correction factor *F* described in the Materials and methods section.

Non-suppression MRI and WASPI experiments were performed on each bone specimen along with the polymer calibration phantom and the marrow tube. Fig. 1 shows typical non-suppression MRI and WASPI images of the calibration phantoms, and the trabecular and cortical bone specimens. In non-suppression MRI (Fig. 1a, c, e), the liquid-state proton signal (water and fat) from bone marrow dominates the image and both the marrow tube and bone specimens are very bright. In the WASPI images, the marrow tube is invisible and the water and fat signals from the bone marrow are suppressed to less than 4% in WASPI (Fig. 1b, d, f). Due to the magnetic susceptibility discontinuity at the fluid-air interface, there is a substantial field gradient present, and a thin superficial layer of marrow signal is not suppressed (Fig. 1b). This susceptibility artifact is greatly alleviated *in vivo* where the bone is surrounded by soft tissue. The WASPI signal of the rat bone (Fig. 1d, f) thus originates from solid bone matrix (collagen, tightly bound water, and other immobile molecules).

In order to evaluate the accuracy of the bone tissue volume *TV* obtained by counting the total voxel number in non-suppression MR images, three tubes of water with known volumes of 0.112, 0.056, and 0.015 cm^3 measured by weighing the water was imaged by non-suppression MRI (Fig. 2a). The total number of voxels above a threshold intensity were obtained for each water tube. These numbers were converted to the volume in cubic centimeter by multiplying by a factor $(FOV/64)^3$. The volumes obtained were plotted against their known volumes and displayed in Fig. 2b. A strong positive correlation (r^2=0.9997) and a slope close to 1 indicate that the volumes measured by non-suppression MRI are very close to the real volumes. The errors of the volumes measured by non-suppression MRI are less than 5%.

The calibration curve that linked the polymer phantom image density obtained from the WASPI image to the actual polymer mass density was obtained for each imaging experiment. WASPI derived bone matrix image density values were converted to polymer equivalent mass density (polymer $g.cm^{-3}$) according to these regression relationships (Fig. 3). The true matrix densities of the bone tissue were obtained as described in the Materials and methods section.

To test the quantitative accuracy of the ^{31}P measurements, five HA phantoms with known HA weights were measured using ^{31}P spectroscopy. The results are shown in Table 2. The ^{31}P T_1 of the reference KPF_6 was 3 times longer than that of HA, resulting in a KPF_6 correction factor *F* 39% larger than that of HA (Table 1). Without T_1 correction, significant errors were observed; however, after T_1 correction, the ^{31}P NMR measurements proved to be very accurate with errors within 5% (Table 2).

Fig. 4 shows the bone mineral densities measured by ^{31}P NMR spectroscopy and gravimetric analysis for the CON, OVX, and NFR groups. The mineral density values obtained by ^{31}P NMR were close to those obtained by gravimetric analysis, which proves the accuracy of

these ^{31}P NMR measurements. For cortical bone specimens, both ^{31}P NMR measurements and gravimetric analysis showed that the BMD of the OVX group was not different from that of the CON group ($p = 0.98$ and 0.97 respectively), yet the BMD of the NFR was 22.1% (by ^{31}P NMR, $p < 0.001$) and 17.5% (by gravimetric analysis, $p = 0.004$) lower than that of the CON group. The BMD of trabecular bone tissue was found to be about 40.5% lower in the OVX group relative to the CON group ($p < 0.001$) by ^{31}P NMR, and 24.6% lower ($p = 0.04$) by gravimetric analysis. Decreased BMD was also found in the trabecular NFR group by both ^{31}P NMR (26.8% lower) and gravimetric analysis (21.5% lower) relative to the CON group; the differences were significant ($p < 0.001$ by ^{31}P NMR and $p = 0.02$ by gravimetric analysis).

Fig. 5 shows the bone matrix densities measured by WASPI and gravimetric analysis for the CON, OVX and NFR groups. No significant changes of cortical bone matrix density in the OVX group were observed by either WASPI or gravimetric analysis relative to the CON group, yet the cortical bone matrix densities in the NFR group were 13.9% lower than that of the CON group by gravimetric analysis ($p = 0.01$) and 10.3% lower by WASPI ($p = 0.06$). On the contrary, although the trabecular bone matrix density in the NFR group was 3.7% lower by WASPI and 12.5% lower by gravimetric analysis relative to the CON group, the decreases are not significant ($p = 0.70$ by WASPI and $p = 0.07$ by gravimetric analysis), yet the trabecular bone matrix densities in the OVX group were 30.8% lower than that of the CON group by gravimetric analysis (p=0.002) and 38.0% lower by WASPI ($p = 0.001$).

The extents of bone mineralization (EBMs) were calculated as the ratio of BMD to bone matrix density from the above measurements (Fig. 6). Although the EBM values of the OVX specimens are somewhat higher than those of the CON group, they are not significantly different. On the contrary, EBMs of the cortical and trabecular specimens were found to be about 12.4% and 26.3% lower in the NFR group relative to the CON group ($p = 0.06$ and $p = 0.02$) by MR, and 4.0% and 11.9% lower ($p = 0.02$ and $p = 0.17$) by gravimetric analysis. Except for the last measurement, these differences are all statistically or marginally significant; the $p = 0.17$ comparison is due to the large standard deviation in the trabecular NFR gravimetry measurement.

Histopathology studies were performed on representative samples from each group after WASPI. Microscopic evaluation revealed morphologic differences in the rat femoral diaphysis bone specimens examined. The control specimen showed normal cortical and cancellous bone with evidence of previous endochondral ossification. The ovariectomized specimen showed a normal cortex with evidence of previous endochondral ossification. With microCT studies on the OVX group, evidence of osteoporosis was found (published elsewhere) [45]. The partially nephrectomized specimen showed evidence of marked osteoclastic activity with cortical cutting cones and significantly resorbed trabeculae. Also present was abundant woven bone formation deposited on the surfaces of the trabeculae and endosteum of the cortex and in the cutting cones. Also noted are several calcospherules within fibrous tissue filling some of the spaces where bone was previously resorbed. These morphologic findings are consistent with severe secondary hyperparathyroidism (Fig. 7).

Discussion

The OVX rat model has been widely used to induce osteoporosis in rat bone. In this study, ^{31}P NMR spectroscopy showed significant decrease of both BMD and bone matrix density in OVX trabecular bone, while the ratio of these two measurements remained similar to that of the CON group, which strongly indicated the presence of osteoporosis: reduced bone mass while the extent of bone mineralization is normal.

The NFR model that has been reported in the literature would create renal insufficiency, disturb the kidneys' metabolic and excretory functions, and lead to renal osteodystrophy. In moderately uremic animals, there appears a form called "mixed" renal osteodystrophy where impaired mineralization is accompanied by a variable degree of osteitis fibrosa (high turnover lesions) [46]. In this study, the histologic evidence showed mixed osteodystrophic lesions and confirmed the presence of secondary hyperparathyroidism. ^{31}P NMR/WASPI measurements were in agreement with these observations: the EBM of both cortical and trabecular bone were lower than that of the CON group, indicating that the bone tissue in the NFR group is under-mineralized; cortical matrix densities in the NFR group were lower than that of the CON group, indicating high turnover lesions. On the contrary, that there were no significant changes of trabecular bone matrix density in the NFR group indicated that the resorbed bone spaces were filled with osteoid.

The total tissue volume of a bone mainly consists of the extracellular calcified matrix (bone substance) and the bone marrow that fills the porous spaces, but does not include the marrow in medullary cavity spaces in cortical bone specimens. In this study, volumetric non-suppression MRI was used to measure the bone tissue volume because non-suppression MRI can capture both the liquid-state proton signal (water and fat) from bone marrow and the solid-state signal from organic bone matrix. Furthermore, the liquid marrow signal of the bone specimen dominates the non-suppression MR images resulting in high signal to noise ratio, hence reducing measurement errors. The bone tissue volume measurement by non-suppression MR involves counting the voxel numbers of the volumetric non-suppression MRI bone specimen image. This method is prone to partial volume artifacts. However, this is a comparative study of specimens with relatively similar sizes, and the partial volume artifacts can be considered to be uniform across the study. Therefore, it can be assumed that the outcome of the study is not significantly affected by partial volume effects.

Both ^{31}P NMR and gravimetric analysis revealed no change in the bone mineral densities of the cortical OVX group and a significant reduction (~23%) in the cortical NFR group. Additionally, mechanical testing of the same OVX and NFR samples showed that the stiffness of the cortical CON group was not different from that of the OVX group, yet it was 62% greater than that of the NFR group. Similarly the yield load of the CON group was not different from that of OVX group, but was 55% greater than that of the NFR group [45]. Since bone strength depends on bone substance density as well as on the mineralization of the bone substance, it is reasonable that this osteoporosis model, in which cortical bone substance density and mineralization did not change significantly, results in only small changes in cortical strength, whereas partial nephrectomy, in which there is a significant loss of mineral, results in reduced cortical strength. In trabecular bone, which is metabolically more labile, both interventions result in significant bone loss and reduced mineral. The observations of reduced mineral are corroborated by μCT measurements of the same bone specimens [45].

WASPI measures the proton signals arising from the solid bone matrix, which includes a portion of collagen protons, tightly bound water, and other motionally restricted molecules in bone matrix but does not include fluid (spectrally resolvable) water and fat. The average WASPI intensity within the bone profiles visualized on non-suppression MR images was calibrated using polymer density reference phantoms and subsequently converted to true bone matrix mass density, which correlates highly with traditionally accepted chemical analysis. As a result, WASPI measurements generate the matrix density of bone tissue in g cm^{-3}. The gravimetric analysis measures the components of bone matrix pyrolyzed at 600°C (dry bone mass – ash mass), which includes the collagen, noncollagenous proteins, and cellular material, as well as tightly bound water that cannot be completely removed under milder drying conditions, but does not include solvent extractable fat or water that is removable under mild

drying conditions. Therefore, WASPI measurements parallel the gravimetric analyses in terms of the chemical constituents measured.

Other laboratories [15–17] have specifically assigned the short-T_2 signal from bone to "bone water", a term whose definition is highly dependent on the specifics of the method by which it is measured. There is no proof at this time that the WASPI signal contains contributions from the macromolecular content of matrix, as opposed to the signal coming exclusively from bone water. However, it is critical to note that proteins in general, and collagen in particular, contain backbone protons with a low degree of molecular motion (and therefore very short T_2 unlikely to be detected in WASPI), as well as side groups, many of which have much higher molecular mobility (for example, arginine, asparagine, isoleucine, and leucine, all of which have multiple single bonds permitting rapid side group reorientation), or which have ionizable OH or NH_2 groups that can participate in proton chemical exchange [47,48]. In a series of articles the laboratory of Torchia has demonstrated with NMR spectroscopy the great extent of motion of collagen side chains leading to significant narrowing of resonances. For example, the ^{2}H, ^{15}N and ^{19}F side group resonances in intact labeled bone tissue harvested from animals raised on isotopically labeled amino acids showed relatively narrow linewidths [49]. This motional narrowing would readily render the corresponding collagen proton resonances visible with WASPI and other techniques with similar short-T_2 capabilities.

The extent of bone mineralization (EBM) is conventionally defined as the weight of bone mineral in unit volume of bone matrix. A closely related definition of EBM is the ratio of bone mineral density (BMD) divided by bone matrix density; this latter ratio can be directly measured with ^{31}P NMR and WASPI as was done in this study. Knowledge of EBM provides important information on compositional changes in bone substance.

It is further noted that our mineral densities measured by ^{31}P NMR and matrix densities measured by WASPI are in good agreement with those obtained by gravimetric analysis, an accepted gold-standard of quantitative measurements of bone mineral and matrix densities. Currently WASPI is one of only a small number of methods that can measure the bone matrix density *in vivo* noninvasively. ^{31}P NMR spectroscopy is naturally suited to measuring mineral content in specimens, which are of limited spatial extent and can be placed completely within the RF coil [50]. Our results highlight the potential of ^{31}P NMR and WASPI as a new nondestructive means to quantify mineral and matrix densities *in vitro*, and potentially *in vivo*, and hence compositional and nanostructural changes associated with metabolic bone disease.

Acknowledgments

This work was supported by a grant from National Institutes of Health (EB004012). MR facilities were supported in part by National Institutes of Health grant P41RR14075 from the National Center for Research Resources, the MIND Institute, and the Athinoula A. Martinos Center for Biomedical Imaging. We thank Dr. Robert M. Neer of Massachusetts General Hospital for helpful discussions and Dr. Melvin J. Glimcher of Children's Hospital Boston for inspiration and guidance during the research and spirited discussions about the manuscript.

References

1. Bone Health and Osteoporosis: A Report of the Surgeon General. 2004.
2. Sartoris, DJ. Quantitative bone mineral analysis. In: Resnick, D., editor. Bone and Joint Imaging. 2. Philadelphia: W.B. Saunders Company; 1996. p. 154
3. Engelke K, Adams JE, Armbrecht G, Augat P, Bogado CE, Bouxsein ML, Felsenberg D, Ito M, Prevrhal S, Hans DB, Lewiecki EM. Clinical use of quantitative computed tomography and peripheral quantitative computed tomography in the management of osteoporosis in adults: the 2007 ISCD official positions. J Clin Densitom 2008;11:123–162. [PubMed: 18442757]

4. Hangartner TN. Thresholding technique for accurate analysis of density and geometry in QCT, pQCT and microCT images. J Musculoskelet Neuronal Interact 2007;7(1):9–16. [PubMed: 17396001]
5. Boutroy S, Bouxsein ML, Munoz F, Delmas PD. In vivo assessment of trabecular bone microarchitecture by high-resolution peripheral quantitative computed tomography. J Clin Endocrinol Metab 2005;90:6508–15. [PubMed: 16189253]
6. Glowacki J, Hurwitz S, Thornhill TS, Kelly M, LeBoff MS. Osteoporosis and vitamin-D deficiency among postmenopausal women with osteoarthritis undergoing total hip arthroplasty. J Bone Joint Surg Am 2003;85-A:2371–2377. [PubMed: 14668507]
7. Golden SH, Robinson KA, Saldanha I, Anton B, Ladenson PW. Clinical review: Prevalence and incidence of endocrine and metabolic disorders in the United States: a comprehensive review. J Clin Endocrinol Metab 2009;94:1853–78. [PubMed: 19494161]
8. Holick MF. High prevalence of vitamin D inadequacy and implications for health. Mayo Clin Proc 2006;81:353–373. [PubMed: 16529140]
9. Kanis JA, Delmas P, Burckhardt P, Cooper C, Torgerson D. Guidelines for diagnosis and management of osteoporosis. Osteoporos Int 1997;7:390–406. [PubMed: 9373575]
10. Lindsay, R.; Cosman, F. Osteoporosis. In: Fauci, A.; Braunwald, E.; Kasper, DK.; Hauser, SL.; Longo, DK.; Jameson, L.; Loscalzo, J., editors. Harrison's Principles of Internal Medicine. 17. New York: McGraw-Hill; 2008. p. 2397
11. McNamara LM, Ederveen AG, Lyons CG, Price C, Schaffler MB, Weinans H, Prendergast PJ. Strength of cancellous bone trabecular tissue from normal, ovariectomized and drug-treated rats over the course of ageing. Bone 2006;39:392–400. [PubMed: 16644297]
12. Bringhurst, F.; Demay, MB.; Krane, SM.; Kronenberg, HM. Bone and mineral metabolism in health and disease. In: Fauci, As; Braunwald, E.; Kasper, DK.; Hauser, SL.; Longo, DK.; Jameson, L.; Loscalzo, J., editors. Harrison's Principles of Internal Medicine. 17. New York: McGraw-Hill; 2008. p. 2365
13. Basha B, Rao DS, Han Z-H, Parfitt AM. Osteomalacia due to vitamin D depletion: a neglected consequence of intestinal malabsortion. Am J Med 2000;108:296–300. [PubMed: 11014722]
14. Robson MD, Gatehouse PD, Bydder GM, Neubauer S. Human imaging of phosphorus in cortical and trabecular bone in vivo. Magn Reson Med 2004;51:888–892. [PubMed: 15122669]
15. Reichert IL, Robson MD, Gatehouse PD, He T, Chappell KE, Holmes J, Girgis S, Bydder GM. Magnetic resonance imaging of cortical bone with ultrashort TE pulse sequences. Mag Reson Imag 2005;23:611–618.
16. Du J, Hamilton G, Takahashi A, Bydder M, Chung CB. Ultrashort echo time spectroscopic imaging (UTESI) of cortical bone. Mag Reson Med 2007;58:1001–1009.
17. Techawiboonwong A, Song HK, Wehrli FW. In vivo MRI of submillisecond T2 species with two-dimensional and three-dimensional radial sequences and applications to the measurement of cortical bone water. NMR Biomed 2008;21:59–70. [PubMed: 17506113]
18. Idiyatullin D, Corum C, Moeller S, Garwood M. Gapped pulses for frequency-swept MRI. J Magn Res 2008;193:267–73.
19. Anumula S, Magland J, Wehrli SL, Zhang H, Ong H, Song HK, Wehrli FW. Measurement of phosphorus content in normal and osteomalacic rabbit bone by solid-state 3D radial imaging. Magn Reson Med 2006;56:946–952. [PubMed: 17041893]
20. Anumula S, Magland J, Wehrli SL, Ong H, Song HK, Wehrli FW. Multi-modality study of the compositional and mechanical implications of hypomineralization in a rabbit model of osteomalacia. Bone 2008;42:405–413. [PubMed: 18053788]
21. Wu Y, Ackerman JL, Chesler DA, Li J, Neer RM, Wang J, Glimcher MJ. Evaluation of bone mineral density using three dimensional solid state phosphorus-31 NMR projection imaging. Calcif Tissue Int 1998;62:512–518. [PubMed: 9576979]
22. Wu Y, Chesler DA, Glimcher MJ, Garrido L, Wang J, Jiang HJ, Ackerman JL. Multinuclear solid state three dimensional MRI of bone and synthetic calcium phosphates. Proc Nat Acad Sci USA 1999;96:1574–1578. [PubMed: 9990066]
23. Wu, Y.; Ackerman, JL.; Chesler, DA.; Wang, JX.; Glimcher, MJ. In vivo solid state ^{31}P MRI of human tibia in 1.5T. Proc Int Soc Magnetic Resonance in Medicine, 7th Int Meeting, Society of Magnetic Resonance in Medicine; Philadelphia, USA. 1999.

24. Wu Y, Ackerman JL, Chesler DA, Graham L, Wang Y, Glimcher MJ. Density of organic matrix of native mineralized bone measured by water and fat suppressed proton projection MRI. Magn Reson Med 2003;50:59–68. [PubMed: 12815679]
25. Wu Y, Dai G, Ackerman JL, Hrovat MI, Glimcher MJ, Snyder BD, Nazarian A, Chesler DA. Water- and fat-suppressed proton projection MRI (WASPI) of rat femur bone. Magn Reson Med 2007;57:554–567. [PubMed: 17326184]
26. Cao H, Ackerman JL, Hrovat MI, Graham L, Glimcher MJ, Wu Y. Quantitative bone matrix density measurement by water- and fat-suppressed proton projection MRI (WASPI) with polymer calibration phantoms. Magn Reson Med 2008;60:1433–1443. [PubMed: 19025909]
27. Miller SC, Wronski TJ. Long-term osteopenic changes in cancellous bone structure in ovariectomized rats. Anat Rec 1993;236:433–441. [PubMed: 8363048]
28. Reddy Nagareddy P, Lakshmana M. Assessment of experimental osteoporosis using CT-scanning, quantitative x-ray analysis and impact test in calcium deficient ovariectomized rats. J Pharmacol Toxicol Methods 2005;52:350–355. [PubMed: 15996488]
29. Yao W, Hadi T, Jiang Y, Lotz J, Wronski TJ, Lane NE. Basic fibroblast growth factor improves trabecular bone connectivity and bone strength in the lumbar vertebral body of osteopenic rats. Osteoporos Int 2005;16:1939–1947. [PubMed: 16086094]
30. Ito M, Nishida A, Aoyagi K, Uetani M, Hayashi K, Kawase M. Effects of risedronate on trabecular microstructure and biomechanical properties in ovariectomized rat tibia. Osteoporos Int 2005;16:1042–1048. [PubMed: 15711780]
31. Hornby SB, Evans GP, Hornby SL, Pataki A, Glatt M, Green JR. Long-term zoledronic acid treatment increases bone structure and mechanic strength of long bones of ovariectomized adult rats. Calcif Tissue Int 2003;72:519–527. [PubMed: 12574877]
32. Ogawa K, Hori M, Takao R, Sakurada T. Effects of combined elcatonin and alendronate treatment on the architecture and strength of bone in ovariectomized rats. J Bone Miner Metab 2005;23:351–358. [PubMed: 16133684]
33. Kaczmarczyk-Sedlak I, Janiec W, Pytlik M, Sliwiński L, Folwarczna J, Cegiela U, Nowińska B, Barnaś M. Effect of administration of etidronate and retinol on bone mechanical properties in ovariectomized rats. Pharmacol Rep 2005;57:203–211. [PubMed: 15886419]
34. Guo XE, Goldstein SA. Vertebral trabecular bone microscopic tissue elastic modulus and hardness do not change in ovariectomized rats. J Orthop Res 2000;18:333–336. [PubMed: 10815837]
35. Wang L, Orhii PB, Banu J, Kalu DN. Effects of separate and combined therapy with growth hormone and parathyroid hormone on lumbar vertebral bone in aged ovariectomized osteopenic rats. Bone 2001;28:202–207. [PubMed: 11182379]
36. Feng JQ, Ward LM, Liu S, Lu Y, Xie Y, Yuan B, Yu X, Rauch F, Davis SI, Zhang S, Rios H, Drezner MK, Quarles LD, Bonewald LF, White KE. Loss of DMP1 causes rickets and osteomalacia and identifies a role for osteocytes in mineral metabolism. Nat Genet 2006;38:1310–1315. [PubMed: 17033621]
37. Turner CH, Owan I, Brizendine EJ, Zhang W, Wilson ME, Dunipace AJ. High fluoride intakes cause osteomalacia and diminished bone strength in rats with renal deficiency. Bone 1996;19:595–601. [PubMed: 8968025]
38. Jokihaara J, Järvinen TL, Jolma P, Kööbi P, Kalliovalkama J, Tuukkanen J, Saha H, Sievänen H, Kannus P, Pörsti I. Renal insufficiency-induced bone loss in associated with an increase in bone size and preservation of strength in rat proximal femur. Bone 2006;39:353–360. [PubMed: 16584934]
39. Miller MA, Chin J, Miller SC, Fox J. Disparate effects of mild, moderate, and severe secondary hyperparathyroidism on cancellous and cortical bone in rats with chronic renal insufficiency. Bone 1998;23:257–266. [PubMed: 9737348]
40. Kazama JJ, Iwasaki Y, Yamato H, Murayama H, Sato M, Gejyo F, Kurokawa M, Fukagawa K. Microfocus computed tomography analysis of early changes in bone microstructure in rats with chronic renal failure. Nephron Exp Nephrol 2003;95:e152–e157. [PubMed: 14694269]
41. Brkovic D, Linke J, Jakse G, Bauss F. Changes in bone structure after augmentation cystoplasty in chronic uraemic rats. BJU Int 2005;95:1066–1070. [PubMed: 15839934]

42. Freesmeyer MG, Abendroth K, Faldum A, Krauss C, Stein G. Comparison of peripheral bone and body axis skeleton in a rat model of mild-to-moderate renal failure in the presence of physiological serum levels of calcitropic hormones. Bone 2001;29:258–264. [PubMed: 11557370]
43. Cory E, Nazarian A, Entezari V, Vartanians V, Mueller R, Snyder BD. Compressive axial mechanical properties of rat bone as functions of bone volume fraction, apparent density and micro-CT based mineral density. J Biomech 2010;43:953–960. [PubMed: 20003979]
44. Ernst, RR.; Bodenhausen, G.; Wokaun, A. Principles of nuclear magnetic resonance in one and two dimensions. Oxford: Clarendon Press; 1987. p. 124
45. Nazarian A, Cory E, Muller R, Snyder BD. Shortcomings of DXA to assess changes in bone tissue density and microstructure induced by metabolic bone diseases in rat models. Osteoporos Int 2009;20:123–132. [PubMed: 18516487]
46. Jablonski G, Klem KH, Attramadal A, Dahl E, Rønningen H, Gautvik KM, Haug E, Gordeladze JO. Surgically induced uremia in rats. I: effect on bone strength and metabolism. Biosci Rep 1993;13:275–287. [PubMed: 8142613]
47. Ghiassi-Nejad M, Torzilli PA, Peemoeller H, Pintar MM. Proton spin-spin relaxation study of molecular dynamics and proteoglycan hydration in articular cartilage. Biomaterials 2000;21:2089–2095. [PubMed: 10966019]
48. Nyman JS, Ni Q, Nicolella DP, Wang X. Measurements of mobile and bound water by nuclear magnetic resonance correlate with mechanical properties of bone. Bone 2008;42:193–199. [PubMed: 17964874]
49. Sarkar SK, Hiyama Y, Niu CH, Young PE, Gerig JT, Torchia DA. Molecular dynamics of collagen side chains in hard and soft tissues. A multinuclear magnetic resonance study. Biochemistry 1987;26:6793–6800. [PubMed: 3427044]
50. Brown CE, Allaway JR, Brown KL, Battocletti JH. Noninvasive evaluation of mineral content of bone without use of ionizing radiation. Clin Chem 1987;33:227–36. [PubMed: 3026685]

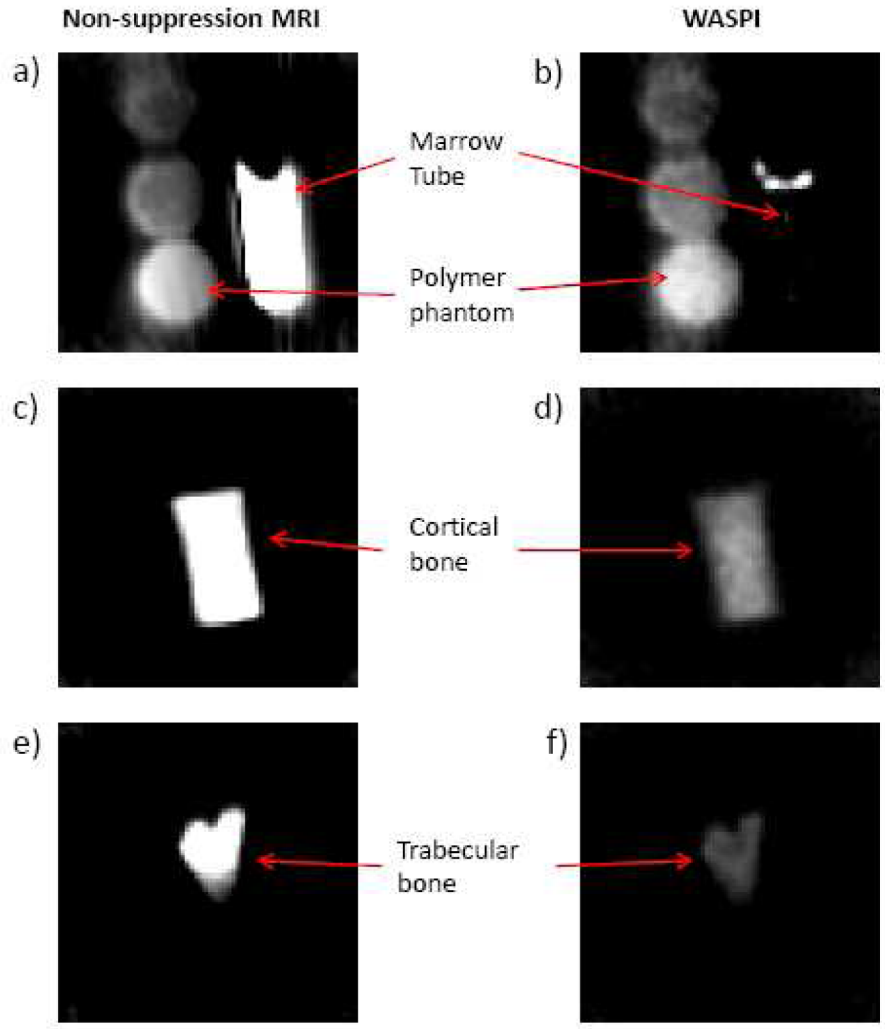

Fig. 1.

Typical non-suppression MRI and WASPI images of rat bone specimens along with three polymer phantoms and bone marrow in a glass tube. a, c, e) Non-suppression MR images. A slice showing three polymer phantoms and bone marrow in a glass tube (a); A slice showing a cortical bone specimen (b); A slice showing a trabecular bone specimen (e). b, d, f) WASPI images corresponding to the subjects in a, c and e.

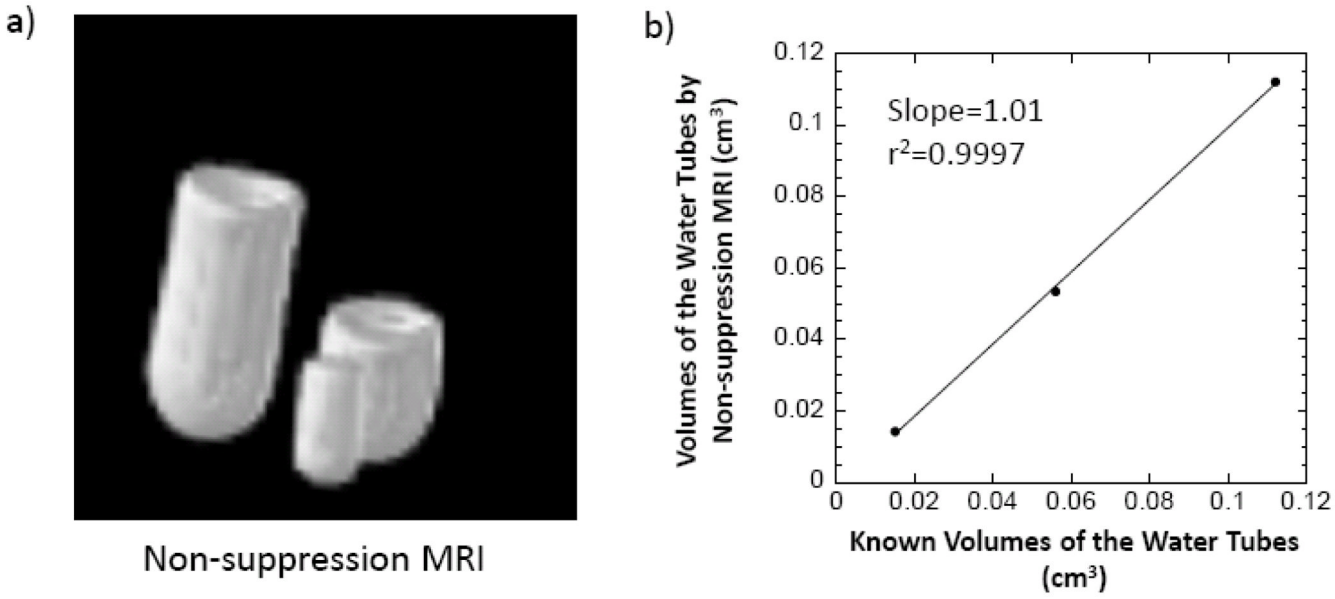

Fig. 2.

Volume calibration using three tubes of water with known volumes of 0.112, 0.056, and 0.015 cm^3, respectively. a) Non-suppression MR images of the three tubes. b) A volume calibration curve plotted as the volumes of the water tubes obtained from the total voxel numbers of the tubes above a threshold in non-suppression MRI vs. their known volumes.

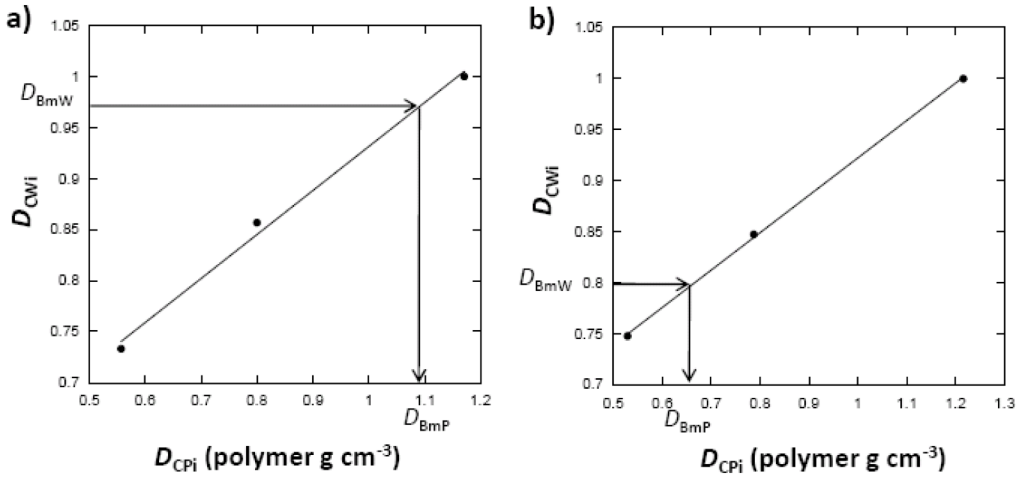

Fig. 3.

Process of obtaining bone matrix densities from WASPI experiments. Calibrations were created by linear regression of the physical densities (D_{cpi}) of the three polymer calibration pellets to their WASPI image densities (D_{cwi}). The arrows denote the process of obtaining the polymer equivalent bone matrix densities (D_{BmP}, expressed in terms of polymer g.cm^{-3}) of the rat bone specimens from their WASPI image densities (D_{BmW}) using the linear regression coefficients. a) Rat normal cortical bone specimen. b) Rat normal trabecular bone specimen. The polymer equivalent bone matrix densities D_{BmP} were then converted to true bone matrix mass densities D_{WmaT} (refer to the text).

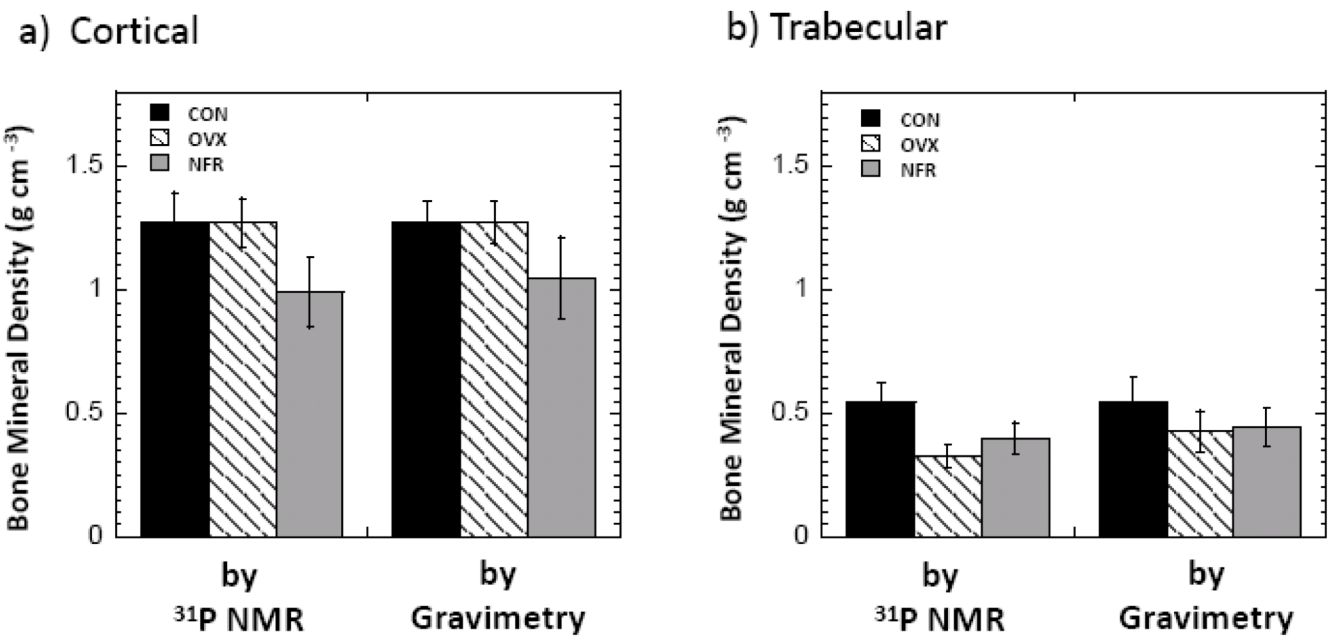

Fig. 4.

Bone mineral densities of the rat bone specimens from CON, OVX, and NFR groups measured by ^{31}P NMR spectroscopy and gravimetric analysis. Bars indicate mean ± SD. a) Cortical. b) Trabecular.

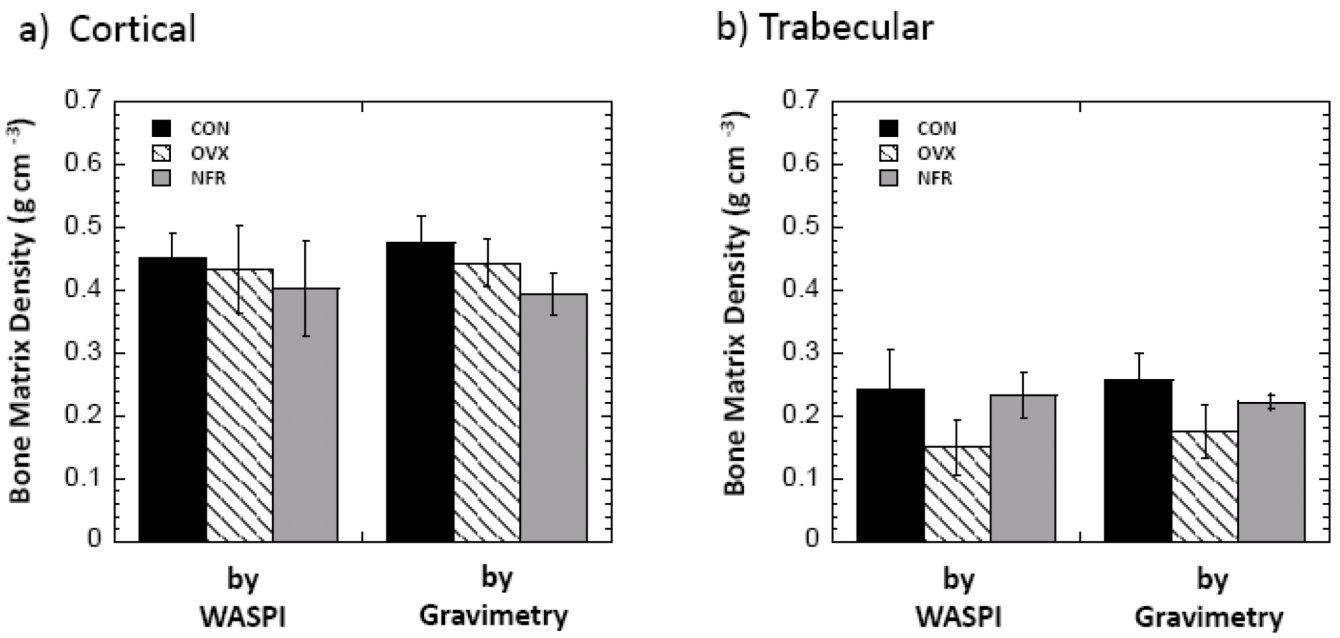

Fig. 5.

Bone matrix densities of the rat bone specimens from CON, OVX, and NFR groups measured by WASPI and gravimetric analysis. Bars indicate mean ± SD. a) Cortical. b) Trabecular.

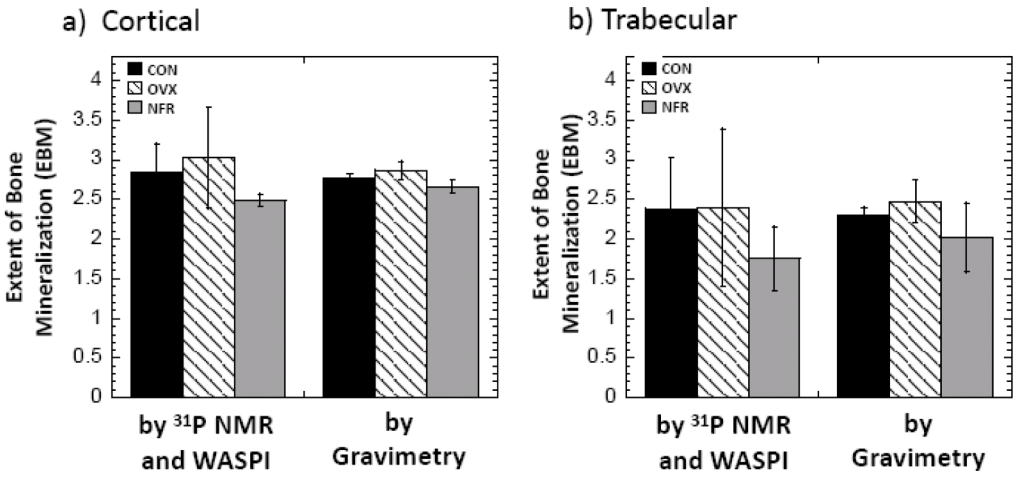

Fig. 6.

The extents of bone mineralization (EBM), calculated as the ratios of bone mineral density to bone matrix density, of the rat bone specimens from CON, OVX, and NFR groups. Bars indicate mean ± SD. a) Cortical. b) Trabecular.

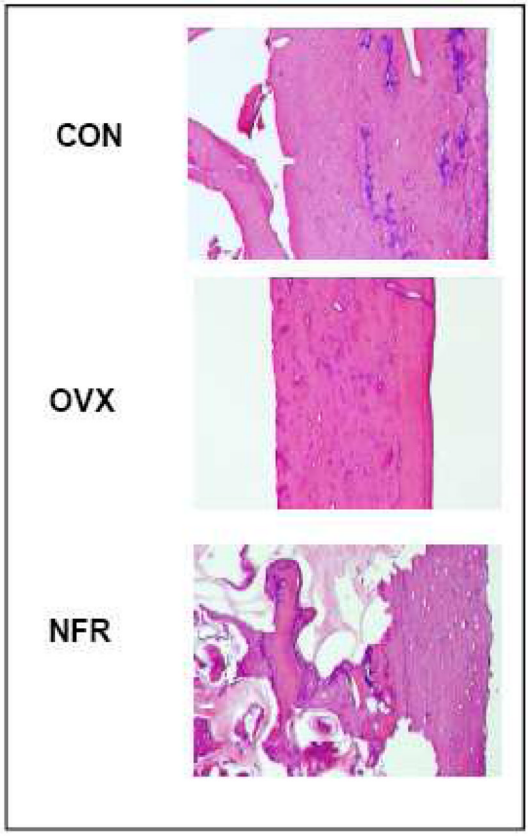

Fig. 7.
Histology study of the rat bone samples from CON, OVX, and NFR groups.

Table 1

Spin-lattice relaxation times T_1 of the protons in polymer blend and rat bone specimens, and ^{31}P spins in hydroxyapatite (HA), KPF_6 and rat bone specimens at 4.7 T. Excitation pulse β was obtained from the fitting of equation 1.

	20% PEO/PMMA	Trabecular	Cortical
^{1}H T_1, s	3.6	3.5	3.6
Excitation pulse β (°)	12	13	13
TR, s	0.15	0.15	0.15
F	7.28	7.05	7.12

	HA	KPF_6	Trabecular			Cortical		
			Normal	NFR	OVX	Normal	NFR	OVX
^{31}P T_1, s	2.7	8.1	27.0	33.8	35.1	51.1	46.9	62.3
Excitation pulse β (°)	20.3	21.5	19.3	19.2	19.3	25.1	19.2	25.9
TR, s	1.0	1.0	1.0	1.0	1.0	1.0	1.0	1.0
F	3.28	4.18	7.53	8.67	8.91	13.62	10.89	16.48

Table 2

Accuracy of ^{31}P NMR spectroscopy measurement of mineral content using five HA phantoms with known mass.

HA known content (g)	HA content by ^{31}P spectroscopy, uncorrected (g)	Error (%)	HA content by ^{31}P spectroscopy, T_1 corrected (g)	Error (%)
0.4217	0.5450	29.23	0.4275	1.37
0.3583	0.4521	26.18	0.3546	−1.02
0.2760	0.3561	29.02	0.2793	1.20
0.2001	0.2675	33.70	0.2099	4.88
0.1629	0.2136	31.11	0.1675	2.85